JCTC Journal of Chemical Theory and Computation

Article

pubs.acs.org/JCTC

Reparametrized E3B (Explicit Three-Body) Water Model Using the TIP4P/2005 Model as a Reference

Craig J. Tainter, Liang Shi, and James L. Skinner*

Theoretical Chemistry Institute and Department of Chemistry, University of Wisconsin, Madison, Wisconsin 53706, United States

ABSTRACT: In this study, we present the third version of a water model that explicitly includes three-body interactions. The major difference between this version and the previous two is in the two-body water model we use as a reference potential; here we use the TIP4P/2005 model (previous versions used the TIP4P water model). We alter four parameters from our previous version of the model by fitting to the diffusion coefficient of the ambient liquid, the liquid and ice densities, and the melting point. We evaluate the performance of this version by calculating many other microscopic and thermodynamic static and dynamic properties as a function of temperature and near the critical point and comparing to experiment, the TIP4P/2005 model and the previous version of our three-body model.

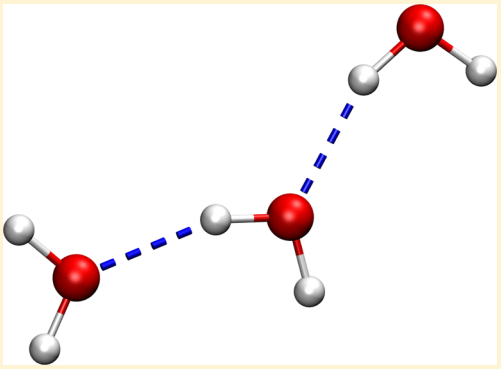

I. INTRODUCTION

Water is an important research topic because of the role it plays in nearly all sciences, as well as its interesting and unusual physical properties. As an example, consider the isothermal compressibility of water at 1 atm pressure, supercooled below its freezing point (273 K). Under normal circumstances one can supercool water down to 232 K, at which point homogeneous nucleation occurs (see, however, ref 1). The compressibility, when extrapolated below 232 K, appears to diverge at 228 K.[2] There is a debate within the community regarding this apparent divergence.[3−5] Some argue that it is a signature of a liquid−liquid critical point hidden in the inaccessible region of the phase diagram.[6] The computational study of a possible liquid−liquid critical point has proven to be very difficult. Several researchers[7−9] have focused on the ST2 model[10] of water since this model relaxes more quickly than most, which makes it easier to achieve metastable equilibrium in the deeply supercooled region. The trade-off, however, is that this model is not a particularly good one for describing experimental water.[10−13]

Some common water models, such as SPC/E[14] and TIP4P,[15] use rigid molecules with fixed charges and assume a pairwise additive form. While popular and generally accurate for many bulk properties, in several studies these models have been reparametrized to obtain better agreement with experiment. For instance, the TIP4P model has been reparametrized for simulations with Ewald summation in TIP4P-Ew,[16] for better prediction of the properties of ice in TIP4P/Ice,[17] as well as a reparameterization for a variety of condensed phases in TIP4P/2005.[18] In fact, the TIP4P/2005 model has proven to be quite remarkable and robust.[19]

It is well-known that in water many-molecule interactions are relatively important.[20−23] Therefore, it must be true that pairwise-additive models incorporate these many-body interactions in some effective or mean-field way. This approach might be expected to work well in homogeneous condensed phases, where the instantaneous molecular environment of a molecule is not that different from the average environment; but in a heterogeneous situation, like at a surface, or near ions or other solutes, this approach would presumably work less well. One way to take these many-body interactions into account approximately is through polarization: allowing the charge distribution of one molecule to respond to the presence of other nearby molecules. Thus, variants of the simple models have been developed by allowing dipoles, charges themselves, or geometry to fluctuate (for some recent examples, see refs 24−31). While these models are very promising, they often require expensive iterative methods to determine self-consistently the fluctuations and/or short time steps to model the vibrations.

An alternative method to treat many-body interactions approximately is to develop a potential surface that includes them explicitly.[25,32,33] It is known that three-body interactions dominate,[20−23] and so it is safe to truncate the expansion at that order. Including three-body interactions might seem like a computational disaster, as then one in principle has to sum over all triplets, but in practice these three-body interactions are very short-ranged, which keeps the computational cost relatively low. We first parametrized a water model with explicit three-body interactions (E3B) in 2008 using TIP4P as the two-body reference potential.[34] While the dynamical properties of TIP4P are generally too fast compared to the experimental measurements, by including these three-body effects, we showed that the dynamics agree better with experiment. Two of the types of three-body interactions are positive—these are called anti-cooperative. A third type is negative—these are called cooperative. In condensed-phase water, with the constraints of

Received: February 6, 2015
Published: March 20, 2015

DOI: 10.1021/acs.jctc.5b00117
J. Chem. Theory Comput. 2015, 11, 2268−2277

its near-tetrahedral hydrogen bonding, both cooperative and anticooperative interactions are prevalent. Our view is that some of the interesting properties of condensed-phase water arise from the local competition between cooperative and anticooperative interactions.

We later determined that the E3B model had some faults. The model was parametrized in the microcanonical (NVE) ensemble. From subsequent NpT simulations we discovered that the liquid density at 298 K and atmospheric pressure was too low compared to experiment. The model was then reparametrized (hereafter called E3B2) to ensure that the correct density was obtained.[35] At the same time, we decided to focus on fitting to a wider range of experimental properties including the surface tension and the melting point. We have used this version quite extensively to examine the structure of water at the liquid/vapor interface,[36,37] the water hexamer,[38,39] the dielectric constant and THz spectroscopy of liquid water and ice Ih,[40] and OH-stretch spectroscopy of water and ice Ih.[41,42] We also discussed a new approach to modeling monovalent salts in aqueous solution in the context of this model.[43]

There are two circumstances for bulk water where large density fluctuations exist, and hence the system is locally heterogeneous, and three-body effects may be more important. One is near the critical point, where one understands that there are density fluctuations on all length scales.[44] Moreover, for hydrogen-bonded systems like water, near the critical point clusters of hydrogen-bonded molecules are expected to be quite stringy or ramified. It is precisely in this situation where three-body interactions might be quite important, because the competition we alluded to above between cooperative and anticooperative interactions might be settled more in favor of the cooperative interactions when the density is lower (the density near the critical point is about one-third of the liquid density) and the hydrogen-bonding coordination is lower. The second situation is in deeply supercooled water, where there may be regions of high and low density,[45,46] signaling the possible presence of the nearby liquid−liquid critical point. In fact, two works have explicitly speculated about the special importance of three-body interactions for supercooled water.[47,48]

The E3B2 model has a melting temperature (at 1 atm) of 251 K (compared to 273 K in experiment) and a critical temperature of 570 K (compared to the experimental value of 647 K). In order to compare directly to experiment for supercooled and supercritical water, we would prefer to have a model with better melting and critical temperatures. This is the impetus for the present third parametrization of the E3B model. As noted above, for the first two versions of our model we used the TIP4P model as a two-body reference, which has melting and critical temperatures of 232 and 588 K, respectively.[49] In contrast, the TIP4P/2005 model has melting and critical temperatures of 252 and 640 K, respectively. Since these are close to experiment, and TIP4P/2005 is considered to be the best available rigid two-body model, our thinking was that for this third effort we should use this model as our two-body reference, which is what we do herein. The outline of the paper is as follows. In section II we review the form of the potential as well as the parametrization scheme. We present the results of the fit properties as well as many additional properties in section III and conclude in section IV.

II. POTENTIAL DEVELOPMENT

A. Form of the Potential. We begin with an overview of the form of the E3B potential. The total potential energy of any system can be divided into terms that depend on two molecules, three molecules, etc. Truncating this expansion at the three-body term yields

$$U = \sum_i \sum_{j>i} E_{ij} + \sum_i \sum_{j>i} \sum_{k>j} \Delta E_{ijk} \tag{1}$$

where U is the total potential energy, the first term on the right-hand side represents the two-body potential energy and the second term is the additional energy arising solely from each collection of three molecules (that is, it excludes pairwise energies). Electronic-structure calculations have shown that two- and three-body interactions are responsible for the majority of the binding energy in water clusters.[20−23]

Pairwise models, such as TIP4P/2005, are more appropriately described as *effective* two-body potentials, since they are parametrized from experiment and therefore must take into account many-body interactions implicitly. Since we want to use TIP4P/2005 as the two-body reference, our strategy is to remove the effective many-body interactions with a two-body correction, and then add them back in with explicit three-body interactions. Thus, the two-body potential energy for molecules i and j is written as[35]

$$E_{ij} = E_{ij}^{\mathrm{TIP4P/2005}} + E_2 e^{-k_2 r_{ij}^{OO}} \tag{2}$$

where the correction, given by the second term on the right-hand side of eq 2, depends only on the distance between the oxygen atoms of the two molecules.[35] Here, E_2 will be one of the fitting parameters, while we will keep k_2 equal to the value found in E3B2 (see below). Note that since the net effect of the three-body interactions is negative, the two-body correction is positive, and so $E_2 > 0$.

We have parametrized the three-body interactions based on intermolecular O···H distances.[34,35] Specifically, for each triplet of molecules, we consider all the ways that the molecules are "connected" by two O−H distances. There are 42 such ways, which fall naturally into three types, differentiated by which atoms of the "bridging" molecule are involved. Type A interactions are those in which each hydrogen on the bridging molecule is involved, type B interactions are those in which a hydrogen and the oxygen on the bridging molecule are involved, and type C interactions are those in which the oxygen atom on the bridging molecule is involved twice. See Figure 1 of ref 35 for a schematic of each type.

A hydrogen bond between two water molecules involves a small amount of charge transfer,[50] from the lone-pair electrons of the "acceptor" oxygen to the σ^* OH antibonding orbital of the "donor" hydrogen. In type A interactions, which arise from acceptor−donor−donor−acceptor configurations, the charge transfer in one hydrogen bond diminishes the amount of charge transfer in the other, thus weakening the second hydrogen bond. Thus, we call this an anticooperative interaction. One can also think of this as arising from charge excess on the bridging molecule. In type C, donor−acceptor−acceptor−donor interactions, the charge transfer in one hydrogen bond also diminishes the amount of charge transfer in the other, and so this is also an anticooperative interaction. This arises from a charge deficit on the bridging molecule. However, in type B interactions, which arise from donor−acceptor−donor−acceptor configurations, charge transfer in one hydrogen bond enhances the amount of charge transfer in the other, thus strengthening the second hydrogen bond. We call this a cooperative interaction.

We write the three-body potential energy of trimer ijk as

DOI: 10.1021/acs.jctc.5b00117
J. Chem. Theory Comput. 2015, 11, 2268−2277

$$\Delta E_{ijk} = \Delta E^{A}_{ijk} + \Delta E^{B}_{ijk} + \Delta E^{C}_{ijk} \quad (3)$$

where ΔE^{A}_{ijk} represents the sum of the 6 type A interactions, ΔE^{B}_{ijk} represents the sum of the 24 type B interactions, and ΔE^{C}_{ijk} represents the sum of the 12 type C interactions. Figure 3 and eqs 7−9 of ref 34 explicitly define all 42 terms. The form for each three-body interaction is given by

$$f(r_1, r_2) = E_A \cdot \exp[-k_3(r_1 + r_2)]$$
$$g(r_1, r_2) = E_B \cdot \exp[-k_3(r_1 + r_2)]$$
$$h(r_1, r_2) = E_C \cdot \exp[-k_3(r_1 + r_2)] \quad (4)$$

where r_1 and r_2 are the two O···H distances. Here, f, g, and h represent the form for types A, B, and C, respectively. E_A, E_B, and E_C are adjustable parameters, and we will again keep the k_3 parameter identical to the E3B2 model.[35] As per the above discussion, we find that E_A, $E_C > 0$, and $E_B < 0$.

Since our three-body interactions are short-ranged (they decay exponentially), we would like to truncate them smoothly. To this end we multiply the functions in eq 4 by the product $s(r_1)s(r_2)$, where the switching function $s(r)$ is given by

$$s(r) = \begin{cases} 1 & \text{if } (r < r_s) \\ \dfrac{(r_f - r)^2(r_f + 2r - 3r_s)}{(r_f - r_s)^3} & \text{if } (r_s \le r \le r_f) \\ 0 & \text{if } (r > r_f) \end{cases} \quad (5)$$

and we set r_s to be 5.0 Å and r_f to be 5.2 Å. The factor $s(r_1)s(r_2)$ switches off the three-body potential energies and forces if r_1 or r_2 is more than 5.2 Å.

B. Parameterization Scheme. As stated in the previous section, we decided to keep the decay parameters k_2 and k_3 equal to the values found in E3B2. We realized that including more parameters was not necessarily advantageous considering that certain parameters are *correlated* to one another. For instance, increasing the exponential decay parameter (k_2 or k_3) has roughly the same effects on the model's properties as decreasing the magnitude of the corresponding pre-exponential factor (E_2 or E_A, E_B, and E_C) with the original decay parameter. In this parametrization, we decided to focus on fitting the diffusion coefficient (D) at ambient conditions, the liquid density (ρ_l) at 298 K, the solid density (ρ_s) at 273 K, and the melting temperature (T_m) at atmospheric pressure. The goal then is to minimize the function

$$\chi^2 = \sum_n w_n (P_n - P_n^{expt})^2 \quad (6)$$

where the summation runs over the properties being fit, w_n are weights given each property, and P_n is the value of property n produced by the model. The weights reflect our judgment as to the relative importance of each property.

Even with only four parameters, it is not feasible to search over all of parameter space. We therefore proceed with a two-step approach to arrive at the final parameter set. In the first step, we evaluated eq 6 at 121 evenly spaced points in E_2-E_B parameter space. Here, E_2 varied from 0 to 2.5×10^6 kJ/mol in steps of 2.5×10^5 kJ/mol and E_B varied from −5000 to 0 kJ/mol in steps of 500 kJ/mol. At each point, we used the E_A/E_B and E_C/E_B ratios of −0.4 and −1.7, respectively. These values are approximately the same as the final parameters in E3B2 and represent a good balance between anticooperative and cooperative three-body interactions.

Step 2 started with the parameter set that gave the smallest χ^2 value from step one. Let us define this point as $\{E_2^0, E_A^0, E_B^0, E_C^0\}$. We then calculated the fitting properties at 81 parameter sets given by $\{E_2^0 + m_2 \cdot \Delta E_2, E_A^0 + m_A \cdot \Delta E_A, E_B^0 + m_B \cdot \Delta E_B, E_C + m_C \cdot \Delta E_C\}$ where each m takes on the values of −1, 0, or 1. Here we used $\Delta E_2 = 1.25 \times 10^5$ kJ/mol and $\Delta E_A = \Delta E_B = \Delta E_C = 250$ kJ/mol. For each property P_n, we can construct a polynomial function of the form

$$P_n(E_2, E_A, E_B, E_C) = \sum_{i=0}^{2}\sum_{j=0}^{2}\sum_{k=0}^{2}\sum_{l=0}^{2} C^n_{ijkl} (E_2)^i (E_A)^j (E_B)^k (E_C)^l \quad (7)$$

where the 81 C^n_{ijkl} coefficients can be uniquely determined for each property by fitting to the values of property n at the 81 parameter sets mentioned above. This function exactly interpolates between the values of the properties at all 81 parameter sets and provides a means to predict the values of the properties in the parameter space defined by $E_\xi^0 - \Delta E_\xi \le E_\xi \le E_\xi^0 + \Delta E_\xi$ ($\xi = 2, A, B, C$). We use eq 7 to predict the properties and thus are able to fine-tune the parameters by finding where eq 6 is minimized. This method was in fact very accurate, and we were not able to improve the properties after a single iteration.

C. Simulation Details. All simulations were performed using version 4.5.5 of the GROMACS simulation package, which was modified to include the three-body interactions.[51−54] All simulations used 500 water molecules except for the ice Ih simulations, which had 432 molecules. The initial proton-disordered ice Ih structure was generated according to Hayward and Reimers, such that each molecule accepted and donated two hydrogen bonds while minimizing the total dipole moment.[41,55−58] In all of the systems, the equations of motion were integrated using the leapfrog algorithm with a 1 fs time step. The temperatures were held constant at the appropriate value using the Nosé−Hoover thermostat with a coupling time of 5 ps.[59,60] For the constant-pressure simulations, we used the Parrinello−Rahman barostat with a coupling time of 10 ps.[61] The Lennard-Jones potential was cut off at a distance of 1.0 nm, and standard corrections were applied to the energy and pressure.[62] Ewald sums were used to treat the electrostatic interactions. The real-space part of the Coulombic potential was cut off at 1.0 nm. The reciprocal-space part was evaluated using the Particle-Mesh Ewald method.[63] The mesh width was set to 0.12 nm, and a fourth-degree polynomial was used. Constraints were used to keep the molecules in the TIP4P/2005 geometry.[64]

All of the bulk-liquid properties were calculated from 20 ns NpT simulations. All of the properties of supercritical water were calculated from 10 ns NpT simulations, before which NVT simulations were performed to estimate the pressures required for the desired densities (i.e., 0.1, 0.2, ..., 1.0 g/mL).

The surface tension was calculated using a 20 ns NVT slab simulation. The density of ice was determined using a 1 ns NpT simulation. For the calculation of the melting point, separate 300 ps liquid and ice NpT simulations were used. Finally, the simulations needed for the critical point were determined using 1 ns NpT simulations for the liquid and 2 ns NpT simulations for the vapor. We note that we extended the Lennard-Jones and Coulombic cutoffs to 5.0 nm for the vapor simulations.

DOI: 10.1021/acs.jctc.5b00117
J. Chem. Theory Comput. 2015, 11, 2268−2277

III. RESULTS

The final E3B3 parameters are given in Table I. Note that k_2 and k_3 were not reparametrized in this paper and are simply presented for completeness. It is interesting to note that all of the new pre-exponential factors are smaller than they were for E3B2.[35] This is not completely surprising considering that TIP4P/2005 is a better reference potential than TIP4P, and thus the "magnitude" of the terms added on (two-body correction and three-body terms) is smaller.

Table I. Final E3B3 Parameters

parameter	value
E_2	0.453×10^6 kJ/mol
k_2	4.872 Å^{-1}
E_A	150.0 kJ/mol
E_B	−1005.0 kJ/mol
E_C	1880.0 kJ/mol
k_3	1.907 Å^{-1}

Before we proceed, we wish to mention that many of the properties calculated below were calculated for E3B2; we refer the reader to ref 35 for details on how to perform these calculations. The procedures for other properties are described below. The results for the properties used in the fitting procedure are given in Table II, and the results for some other properties are given in Table III. For all properties except for those of supercritical water, we compare to the TIP4P/2005 and E3B2 models and to experiment.

Table II. Values of Properties Used in the Fit of E3B3

model	D (298 K) (10^{-5} cm^2/s)	ρ_l (298 K) (g/mL)	ρ_s (273 K) (g/mL)	T_m (K)
E3B2	2.27	0.993	0.935	251
TIP4P/2005	2.32	0.999	0.917	252[18]
E3B3	1.98	0.993	0.918	260
expt	2.29[89]	0.997[90]	0.917[91]	273[91]

A. Diffusion Coefficient. The diffusion coefficient, D, at 1 atm and 298 K was used to fit the potential (and the value is listed in Table II). This value is lower than the experimental number[65] by some 15%, and is clearly worse than the results for the E3B2 and TIP4P/2005 models. This discrepancy can be attributed to the fact that we gave the diffusion coefficient a smaller weight in eq 6 above. We thought it was more important to obtain more accurate liquid and solid densities as well as a better melting point, and this led to a smaller diffusion coefficient compared to experiment.

The diffusion coefficient as a function of temperature over the entire liquid range is shown in Figure 1. The agreement with experiment[65] is reasonably good for all models (D increases dramatically as T increases) but is slightly better for the E3B2 and TIP4P/2005 models.

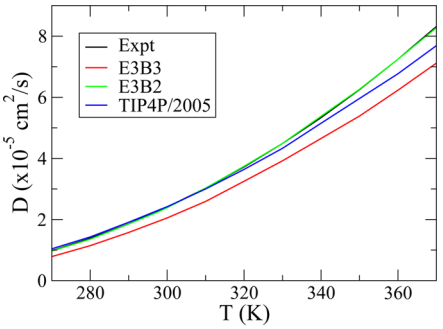

Figure 1. Diffusion coefficient for liquid water at 1 atm as a function of temperature for the E3B3, E3B2, and TIP4P/2005 models as compared to experiment.[65]

We should note that the diffusion coefficient calculated from molecular dynamics simulations depends on the system size, and a correction is usually added to extrapolate to infinite box size.[66−68] This correction is inversely proportional to the viscosity. In ref 35, we used the experimental value of the viscosity, while in this study, we used the viscosity that is calculated for each model at each temperature (see section I).

B. Melting Point. The melting point (T_m) for all of the models is given in Table II. Most classical force fields for water underestimate the melting point. E3B2 did an excellent job of improving the melting point over that of the TIP4P reference potential (232 K). Here, with the TIP4P/2005 model as the reference, we were again able to improve upon the melting point—our value for E3B3 is 260 K. Throughout the parametrization, we encountered parameter sets that did have higher melting points, but these models also had smaller diffusion coefficients.

C. Liquid and Solid Densities. We used the liquid density, ρ_l, at 1 atm and 298 K to fit the potential, and the value is shown in Table II. It is in excellent agreement with experiment, as it is for the other models. We also used the density of ice Ih, ρ_s, at 1 atm and at the experimental melting point of 273 K. The results for all the models are presented in Table II. The solid density for E3B2 was significantly higher than experiment even though it was one of the properties that was fit. Here, we see that both TIP4P/2005 and E3B3 have solid densities in much better agreement with experiment than the density for E3B2.

The liquid density as a function of temperature is shown in Figure 2. Here we see that TIP4P/2005 does the best job of matching experiment. E3B3 slightly underestimates the density at all temperatures, while E3B2 is off by a couple of percent at higher temperatures. We determine the temperature of maximum density (T_{MD}) by fitting a polynomial to the data for each model. T_{MD} for each model is given in Table III. TIP4P/2005 is very accurate for this property, as it was used in determining the parameters for this model. E3B3 overestimates the temperature of maximum density (by 6 K), while E3B2 underestimates it (by 9 K).

Table III. Values of Other Properties Calculated in This Study

model	T_{MD} (K)	γ (mN/m)	ΔH_v (kcal/mol)	T_c (K)	ρ_c (g/mL)	p_c (bar)	T_b (K)
E3B2	268	62.3[35]	10.50	570	0.295	137	361
TIP4P/2005	278[18]	69.3[92]	11.00	640[49]	0.310[49]	146[49]	401[49]
E3B3	283	69.9	11.14	626	0.335	143	400
expt	277[69]	72[92]	10.52[15]	647[49]	0.322[49]	221[49]	373.15[49]

DOI: 10.1021/acs.jctc.5b00117
J. Chem. Theory Comput. 2015, 11, 2268−2277

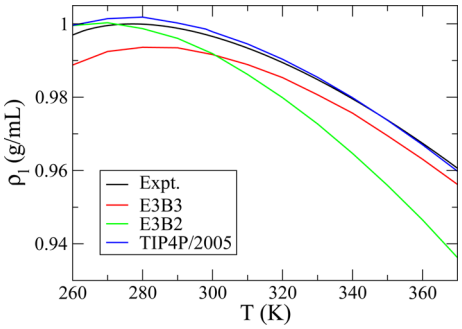

Figure 2. Liquid density at 1 atm as a function of temperature for the E3B3, E3B2, and TIP4P/2005 models as compared to experiment.[90]

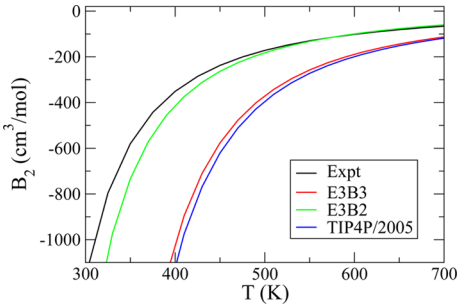

Figure 3. Second virial coefficient as a function of temperature for the E3B3, E3B2, and TIP4P/2005 models as compared to experiment.[93]

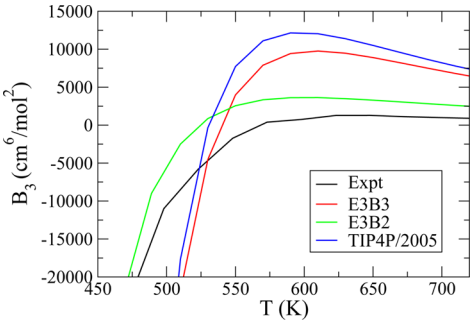

Figure 4. Third virial coefficient as a function of temperature for the E3B3, E3B2, and TIP4P/2005 models as compared to experiment.[94]

We now wish to mention the work of Vega and Abascal, in which they find that for simulation models T_{MD} is often more than 20 K higher than T_m[69] (in experiment it is only 4 K higher). They state that the location of the negative charge within the molecule has a large influence on the difference between T_m and T_{MD}. It appears that even with the inclusion of the three-body interactions this is still the case. We did not calculate $\rho(T)$ for any parameter sets besides the final ones, however, to test if three-body interactions can change the relationship between T_m and T_{MD}.

D. Surface Tension. The surface tension, γ, of each model at 298 K is given in Table III. Both E3B3 and TIP4P/2005 are in very good agreement with experiment, while E3B2 slightly underestimates the surface tension. Surface tension was used in the parametrization of E3B2. As we stated in ref 35, the surface tension of E3B2 is lower than experiment because we gave higher weights to other fitting properties. We observed that the liquid density and surface tension are positively correlated such that larger values of surface tension would increase the liquid density above the experimental value. We did not use the surface tension as a fitting property for E3B3 under the assumption that it would also correlate with the liquid density. This turned out to be the case, and the results are in good agreement with experiment. This is perhaps not too surprising considering the good agreement between the reference TIP4P/2005 potential and experiment.

E. Enthalpy of Vaporization. The enthalpy of vaporization, ΔH_v, at 298 K is presented in Table III. TIP4P/2005 and E3B3 both overestimate this property, while E3B2 is in very good agreement with experiment. Abascal and Vega stated in the original TIP4P/2005 paper that it is not possible to obtain good values of both the melting temperature and the vaporization enthalpy at the same time. Thus, their final model parameters were chosen to balance these properties. We make a very similar observation with E3B3. Here, we prioritized the melting point in our parametrization, and, as such, the enthalpy of vaporization is slightly worse.

F. Second and Third Virial Coefficients. The second and third virial coefficients are particularly interesting when evaluating the quality of intermolecular potentials because they directly probe the potential for two and three molecules, respectively. Here, we present the second and third virial coefficients compared to experiment in Figures 3 and 4. Note that even though E3B3 is in better agreement with experiment compared to TIP4P/2005, the changes in the virial coefficients are fairly small. This is simply because the magnitude of the two-body correction and three-body terms are small compared to those in E3B2. The virial coefficients of E3B2 improved substantially compared to the reference TIP4P potential (as shown in ref 35) because the pre-exponential coefficients E_2, E_A, E_B, and E_C are large compared to those of E3B3. Thus, although it is unfortunate that E3B3 is not as good at reproducing the second and third virial coefficients as E3B2, it is also somewhat expected. This provides some insight into what is needed to create a robust potential for water. While TIP4P/2005 reproduces many condensed-phase properties, it is not as accurate in computing gas-phase properties.[38,70,71]

G. Vibrational Density of States. The vibrational density of states (VDOS) is very helpful in understanding vibrational dynamics in condensed phases. The intermolecular vibrations in water are dominated by hydrogen motions, hence the VDOS in water can be estimated by the Fourier transform of the (classical) hydrogen velocity time-correlation function (TCF), given by

$$f(\omega) = \frac{1}{2\pi}\int_{-\infty}^{\infty} \mathrm{d}t\ \mathrm{e}^{-i\omega t}\langle \vec{v}(0)\cdot\vec{v}(t)\rangle \tag{8}$$

where $\vec{v}(t)$ is the classical hydrogen velocity, and the brackets denote a classical equilibrium ensemble average. $f(\omega)$ can be obtained from inelastic incoherent neutron scattering.

In Figure 5, the calculated and experimental[72,73] $f(\omega)$ are shown for liquid water at about 300 K. The agreement between experiment and theory is reasonable for all three water models: the translational peak at about 50 cm^{-1}, which is often assigned to O···O···O intermolecular bending modes, and the librational peak around 550 cm^{-1} (the hindered rotation of water molecule) are well reproduced at about the right positions (the librational peak in theory is too blue by about 50 cm^{-1}), although the relative intensity between these two peaks is not so good in the simulation. The reason for the discrepancy in intensity is unclear but is unlikely to arise from nuclear quantum effects: if one applies a so-called quantum correction factor[74] to incorporate nuclear quantum effects into $f(\omega)$ phenomenologically, the higher-frequency librational peak will be further enhanced.[75] In

DOI: 10.1021/acs.jctc.5b00117
J. Chem. Theory Comput. 2015, 11, 2268−2277

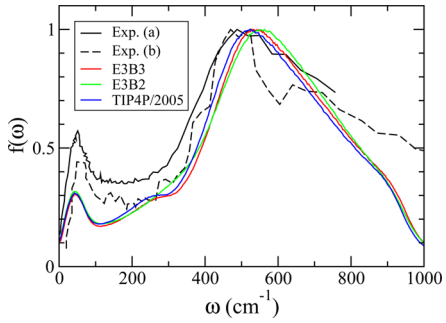

Figure 5. Calculated vibrational density of states (i.e., Fourier transform of the hydrogen velocity time-correlation function) of liquid water at 300 K and 1 atm from eq 8 for the E3B3, E3B2, and TIP4P/2005 models and experimentally extracted results. Exp (a) is at 298 K from ref 72, and Exp (b) is at 300 K from ref 73.

fact, we did not apply a quantum correction factor for $f(\omega)$ since the diffusion coefficient and H−H rotational correlation time of water are well reproduced by these classical models, implying perhaps that nuclear quantum effects are implicitly included during their parametrizations against experimental data (see refs 76 and 68 for a comparison between these dynamic properties calculated from classical and quantum simulations for liquid water).

Among the three models, E3B3 and TIP4P/2005 give very similar results, and both also predict a shoulder/peak at about 250 cm^{-1}, which is not seen in the VDOS from E3B2. The existence of this feature in the experimental VDOS is difficult to confirm due to the noise in experiment. However, this feature is more pronounced in the experimental low-frequency IR spectrum of liquid water and is often attributed to the hydrogen-bond stretching mode.[40,77] In comparing E3B3 and its reference potential TIP4P/2005, we find that the VDOS from E3B3 is blue-shifted by about 10 cm^{-1} compared to that from TIP4P/2005, implying that the three-body interactions might make the hydrogen bond network stiffer.

H. Isothermal Compressibility. The isothermal compressibility is calculated (in the NpT ensemble) using the fluctuation formula[78]

$$\kappa_T = \frac{\langle V^2\rangle - \langle V\rangle^2}{k_B T \langle V\rangle} \tag{9}$$

The results for all the models, as a function of T, are shown as the symbols in Figure 6. The solid lines are polynomial fits to the data meant to guide the eye. In comparison to experiment,[79] results for E3B3 are much improved over our previous E3B2 model.

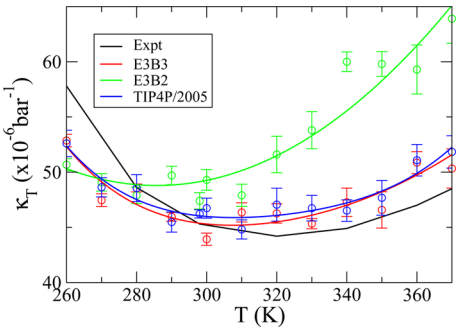

Figure 6. Isothermal compressibility at 1 atm for the E3B3, E3B2, and TIP4P/2005 models and experiment[79] as a function of temperature.

One of the curious features of the compressibility is that it has a minimum (as a functionn of temperature) in the liquid regime (whereas for most other liquids it decreases monotonically as temperature decreases).[4] The experimental minimum occurs at 319 K.[79] The minima for E3B3 and TIP4P/2005 are both near 307 K and in good agreement with experiment.

I. Shear Viscosity. The shear viscosity was calculated using the following time integral[78]

$$\eta = \frac{V}{k_B T}\int_0^\infty \langle \delta P_{\alpha\beta}(t)\delta P_{\alpha\beta}(0)\rangle \mathrm{d}t \tag{10}$$

where $\delta P_{\alpha\beta}$ is the deviation of the off-diagonal elements of the pressure tensor from the average value. The results for all the models, as a function of T, are shown in Figure 7. TIP4P/2005 is

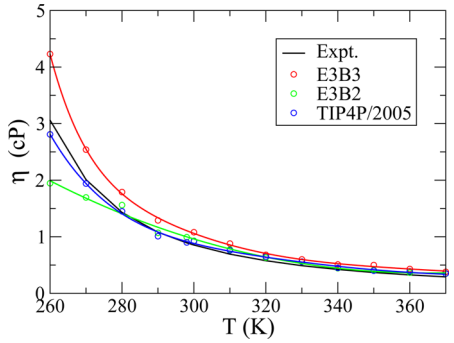

Figure 7. Shear viscosity at 1 atm for the E3B3, E3B2, and TIP4P/2005 models and experiment[95] as a function of temperature.

in the best agreement with experiment. E3B3 and E3B2 begin to overestimate and underestimate this quantity, respectively, as the temperature decreases. Finally, we mention again that the viscosities determined here were used to calculate the finite-size correction to the diffusion coefficient.

J. H−H Rotational Correlation Time. The hydrogen−hydrogen rotational correlation time is a measure of how fast the intramolecular H−H bond vector rotates. We recently showed that E3B2 provides excellent agreement with experiment over a wide range of temperatures for the correlation times of the OH and out-of-plane vectors.[42] There is more limited experimental NMR data for the H−H correlation time.[80,81] In Figure 8 we present the temperature dependence of τ_{HH} for the models in question. At low temperatures, E3B3 clearly overestimates this rotational correlation time; however, the agreement becomes

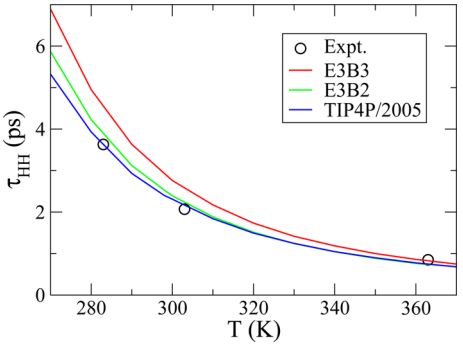

Figure 8. H−H rotational correlation time at 1 atm as a function of temperature for the E3B3, E3B2, and TIP4P/2005 models as compared to experiment.[81]

DOI: 10.1021/acs.jctc.5b00117
J. Chem. Theory Comput. 2015, 11, 2268−2277

better above 320 K. In general, we noticed that the two dynamical properties studied here (D and τ_{HH}) are correlated such that parameter sets that have smaller diffusion coefficients also have a longer H−H rotational time scale.

K. Critical Point and Boiling Point. The method by which we determine the critical point was described by Vega et al. and will be outlined here.[49] We begin by writing

$$U(\alpha) = (1 - \alpha)U^{ref} + \alpha U^{new} \tag{11}$$

where the reference potential, U^{ref}, is a potential for which the critical point is known (TIP4P/2005), and U^{new} is the potential for which we wish to know the critical point (E3B3). The vapor−liquid coexistence pressure changes with the coupling parameter α via the following equation

$$\frac{dp}{d\alpha} = -\frac{(x_v - x_l)}{\tilde{V}_v - \tilde{V}_l} \tag{12}$$

where $\tilde{V}$ is the molar volume, the subscripts denote the vapor and liquid phases, and x is given by

$$x = \langle U^{new} - U^{ref} \rangle_\alpha / N \tag{13}$$

The v-l coexistence pressure of E3B3 at 450 K is first determined by integrating eq 12 from $\alpha = 0$ to $\alpha = 1$. This was achieved by running separate vapor and liquid simulations to determine the terms on the right-hand side of eq 12 and integrating using the Runge−Kutta scheme. Here, we found the v-l coexistence pressure for E3B3 to be 4.52 bar at 450 K.

With this initial coexistence pressure, we calculate the T-p phase diagram by integrating the Clapeyron equation in the form

$$\frac{d \ln p}{d\beta} = -\frac{\Delta \tilde{H}}{p\beta \Delta \tilde{V}} \tag{14}$$

where $\beta = 1/k_B T$, and $\tilde{H}$ is the molar enthalpy. Again, fourth-order Runge−Kutta was used to integrate eq 14, and the temperature was changed in steps of 10 K. Separate vapor and liquid NpT simulations were run to determine the enthalpy and volume changes needed for the right-hand side of eq 14. Repeating this procedure, we were able to map out the vapor−liquid coexistence pressure as a function of temperature. From these simulations, we were also able to determine the densities of the vapor and liquid phases at each temperature and pressure. The v-l phase diagram for the different models are compared to experiment in Figure 9.

The critical temperature can be calculated by employing the Wegner expansion such that the difference between the liquid and vapor densities can be written as[82]

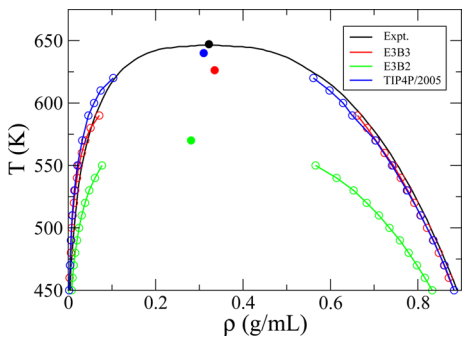

Figure 9. Liquid−vapor coexistence curves for the E3B3, E3B2, and TIP4P/2005 models as compared to experiment.[79,96]

$$\rho_l - \rho_v = A_0|\tau|^{\beta_c} + A_1|\tau|^{\beta_c+\Delta} + A_2|\tau|^{\beta_c+2\Delta} + \ldots \tag{15}$$

where $\tau = 1 - T/T_c$, $\beta_c = 0.325$, and $\Delta = 0.5$. Further, the critical density can be determined from[83]

$$\rho_l + \rho_v = 2\rho_C + D_{1-\alpha}|\tau|^{1-\alpha} + D_1|\tau| + D_2|\tau|^{1-\alpha+\Delta} + D_3|\tau|^{1-\alpha+2\Delta} + \ldots \tag{16}$$

where τ is the same as in eq 15 and $\alpha = 0.11$. In eqs 15 and 16, the coefficients are the fitting parameters. Vega et al. found that four terms in eq 15 and three terms in eq 16 were sufficient to fit the data above 450 K.[49] We follow this procedure and determine that the critical temperature is $T_c = 626$ K for E3B3 (compared to 647 K in experiment). This value of T_c was then used in fitting eq 16, and we find that the critical density for E3B3 is $\rho_c = 0.335$ g/mL. The critical points are depicted in Figure 9 as the solid circles.

The vapor pressure at the critical point can be found by fitting the v-l coexistence pressure (not shown) to Antoine's law[84]

$$\ln(p) = A + \frac{B}{T + C} \tag{17}$$

where A, B, and C are fitting parameters. By inputting the critical temperature into eq 17, one can solve for the critical pressure. Additionally, the normal boiling pressure may be determined by setting $p = 1$ bar and solving for $T = T_b$. The critical pressure and the boiling point are both given in Table III. The results for E3B3 are very similar to those of TIP4P/2005. As anticipated, using TIP4P/2005 as the reference potential for E3B3 has led to a significant improvement of T_c compared to E3B2.

L. Some Properties of Supercritical Water. In this section, some structural, thermodynamic, and dynamic properties of supercritical water (SCW) along the isotherm at 673 K (400 °C) are calculated using the E3B3 and TIP4P/2005 models, and the theoretical results are compared with available experimental data. Note that the E3B2 model is not considered here as its critical temperature (570 K) is significantly lower than the experimental value (647 K).

1. Radial Distribution Functions. The calculated O−O (top panel), O−H (middle panel), and H−H (bottom panel) radial distribution functions (RDFs) at a density of 0.9 g/mL and 673 K using the E3B3 model (red lines) are shown in Figure 10, along with experimental results (black lines) at 0.8733 g/mL and 673 K.[85] Note that experimental RDFs also show intramolecular peaks in O−H and H−H RDFs. The calculated results with the TIP4P/2005 model are not shown here as they largely overlap with the RDFs from the E3B3 model. The agreement and discrepancy between theory and experiment are similar to those often observed for liquid water: the first peak height in the O−O RDF is overestimated by the classical MD simulations with the E3B3 (TIP4P/2005) model, and this overestimation is even more pronounced for the first peak height in the O−H RDF; however, the E3B3 (TIP4P/2005) model surprisingly well reproduces the experimental H−H RDFs.

We also examined the RDFs of SCW at 0.6 g/mL and 673 K, and the calculated results are plotted in Figure 11, along with experimental results at 0.5802 g/mL and 673 K.[85] The agreement is less good than that seen at the higher density, and especially the first peak in the O−O RDF is predicted by the E3B3 (as well as TIP4P/2005) model at 0.29 nm, about 0.03 nm lower than the experimental peak position. This fact might not be surprising since both models are parametrized against water properties at high densities (0.9−1.0 g/mL). As a result, they might tend to describe high-density SCW more properly and might favor high-

DOI: 10.1021/acs.jctc.5b00117
J. Chem. Theory Comput. 2015, 11, 2268−2277

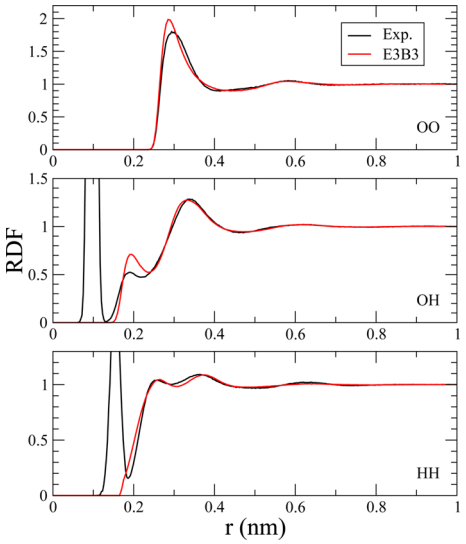

Figure 10. Calculated O−O (top), O−H (middle), and H−H (bottom) radial distribution functions for supercritical water at 673 K and 0.9 g/mL from the E3B3 model (red lines), along with experimental results (black lines) at 673 K and 0.8733 g/mL.[85]

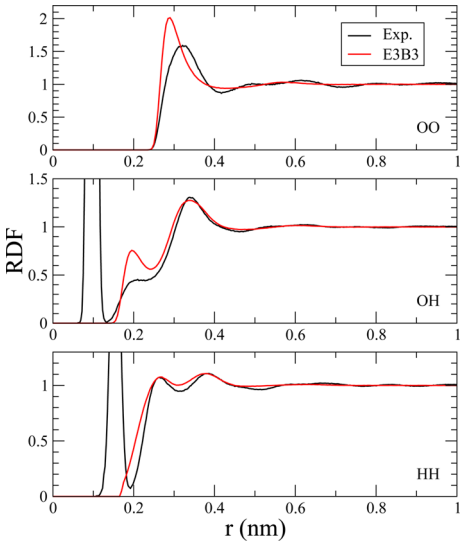

Figure 11. Calculated O−O (top), O−H (middle), and H−H (bottom) radial distribution functions for supercritical water at 673 K and 0.6 g/mL from the E3B3 model (red lines), along with experimental results (black lines) at 673 K and 0.5802 g/mL.[85]

density local structures (clusters) even at intermediate densities, leading to a smaller first-peak position in the O−O RDF.

2. Isothermal Compressibility. Thermodynamic response functions, such as isothermal compressibility κ_T, exhibit extrema with respect to density along isotherms when the temperatures are not very far away from the critical temperature. In Figure 12, the calculated κ_T along the isotherm of 673 K as a function of density for the E3B3 and TIP4P/2005 models is shown. The experimental values are obtained from the empirical formulations released by the International Association for the Properties of Water and Stream (IAPWS-95).[86]

The isothermal compressibility again is calculated from eq 9. Both models reproduce the experimental κ_T fairly well at the densities above 0.4 g/mL but seem to overestimate the response function at lower densities (0.1−0.3 g/mL) although large error

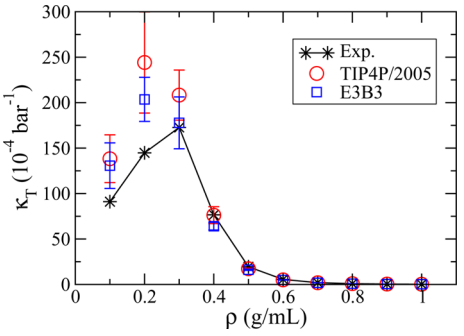

Figure 12. Calculated isothermal compressibility of supercritical water along the isotherm of 673 K as a function of density for the E3B3 and TIP4P/2005 models. Experimental numbers are obtained from the IAPWS Formulation 1995 for General and Scientific Use.[86]

bars are present. This is somewhat surprising in that both models have critical temperatures lower than the experimental one but reasonably good critical densities (cf., Table III), and so the calculated response function would be expected to be smaller compared to the experimental value at the same temperature. However, the observation for κ_T is consistent with what we see in the O−O RDF in Figure 11: both water models tend to generate a tighter and more structured first solvation shell (i.e., smaller peak position and larger peak intensity) for SCW at low densities compared to experiment. The well-known compressibility equation[78] in turn suggests that such models will overestimate κ_T under the same conditions. This once again indicates that water models parametrized from high-density phases (e.g., liquid water and ice) should be used with caution for SCW at low or intermediate densities.

3. Diffusion Coefficient. The diffusion coefficient as a function of density along the isotherm of 673 K is shown in Figure 13. The

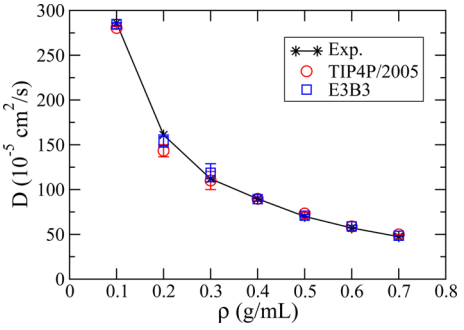

Figure 13. Calculated diffusion coefficient for supercritical water along the isotherm of 673 K as a function of density for the E3B3 and TIP4P/2005 models. The experimental values of shear viscosity[87] is used to correct the finite-size effect. The experimental diffusion coefficients are from ref 88.

experimental viscosity[87] (rather than the calculated viscosity) is used to correct the finite-size effect for the calculated diffusion coefficients. With this correction, both the E3B3 and TIP4P/2005 models reproduce the experiment[88] almost quantitatively. Larger discrepancy is again seen at low densities, albeit at the lowest density (0.1 g/mL) the agreement becomes fairly good again for both models. At very low densities, the kinetic theory of gases[78] might be sufficient to describe the transport properties of SCW (in which case the molecular details become less important).

DOI: 10.1021/acs.jctc.5b00117
J. Chem. Theory Comput. 2015, 11, 2268−2277

IV. CONCLUSIONS

In this paper, we have reparametrized our three-body interaction model using the TIP4P/2005 water model (the best available two-body model) as the two-body reference. Since at this point we are mainly interested in supercooled and supercritical water, our primary goal was to improve the melting temperature (251 K, compared to the experimental value of 273 K) and critical temperature (570 K, compared to the experimental value of 647 K) of our previous version (E3B2). In fact, with this new E3B3 model we are successful in improving the melting and critical temperatures; we obtain 260 and 626 K, respectively. Other properties, like the isothermal compressibility, surface tension, and liquid and ice densities are also better in the new model. However, these improvements come at the expense of some of the dynamical properties (like the diffusion coefficient and the H−H rotational correlation time) and the virial coefficients, which were all described more accurately in the E3B2 version. Thus, for example, like the TIP4P/ice and TIP4P/2005 models, which were parametrized to get different sets of properties more accurately, the choice of the best model depends on what properties one is trying to model.

Our previous three-body water model had six fitting parameters. Here, we use only four fitting parameters by holding the exponential decay parameters k_2 and k_3 fixed at their E3B2 values. One might expect to get better agreement with experiment if more fitting parameters are used; however, in our experience changing the decay parameters leads to corresponding changes in the pre-exponential parameters E_2, E_A, E_B, and E_C, with no overall improvement. Similarly, introducing more parameters, for instance by allowing for different decay parameters for the different three-body terms was something we tried but was not helpful. Finally, we did try other initial E_A/E_B and E_C/E_B ratios, but none led to a better description of the fit properties.

By using the TIP4P/2005 model as the two-body reference, we hoped to be able to improve on the already excellent properties of that model.[19] Our results here are mixed: our melting temperature is better by 10 degrees, but the critical temperature is worse by 14 degreees. Many of the other properties are very similar between the two models. This can be understood since the perturbations (two-body correction and three-body terms) to the reference are substantially smaller for the E3B3 model (compared to the E3B2 model). Therefore, the E3B3 model is actually somewhat similar to the TIP4P/2005 model.

Perhaps the biggest success of the E3B2 model involved the study of the water structure at the liquid−vapor interface, as we briefly mentioned in the Introduction. In fact, we determined that three-body interactions are important to reproduce certain spectroscopic signatures of the molecules at the interface.[37] Results from the pairwise TIP4P/2005 model do not show these features,[37] and so it will be very interesting to see if including the three-body terms as we have done here will lead to agreement with experiment (as with the E3B2 model). This is one direction we have planned for the future.

The biggest payoff of this third reparameterization effort may come from studying microscopic aspects of supercritical and supercooled water. In the former case, the three-body interactions may significantly change the distribution of clusters or even the position of the Widom line. In the case of supercooled water, the three-body cooperative hydrogen-bonding interactions may serve to stabilize more tetrahedral, open, low-density microscopic structures, perhaps consistent with microheterogeneity and the presence of the hidden liquid−liquid critical point. We hope to be able to report on these studies shortly.

AUTHOR INFORMATION

Corresponding Author

*E-mail: skinner@chem.wisc.edu.

Notes

The authors declare no competing financial interest.

ACKNOWLEDGMENTS

We are grateful for support of this work from the National Science Foundation through grant CHE1058752 and from the University of Wisconsin Foundation. We thank Yicun Ni for helpful discussions.

REFERENCES

(1) Sellberg, J. A.; Huang, C.; McQueen, T. A.; Loh, N. D.; Laksmono, H.; Schlesinger, D.; Sierra, R. G.; Nordlund, D.; Hampton, C. Y.; Starodub, D.; DePonte, D. P.; Beye, M.; Chen, C.; Martin, A. V.; Barty, A.; Wikfeldt, K. T.; Weiss, T. M.; Carrona, C.; Feldkamp, J.; Skinner, L. B.; Seibert, M. M.; Messserschmidt, M.; Williams, G. J.; Boutet, S.; Pettersson, L. G. M.; Bogan, M. J.; Nilsson, A. *Nature* **2014**, *510*, 381.
(2) Speedy, R. J.; Angell, C. A. *J. Chem. Phys.* **1976**, *65*, 851.
(3) Mishima, O.; Stanley, H. E. *Nature* **1998**, *396*, 329.
(4) Debenedetti, P. G. *J. Phys.: Condens. Matter* **2003**, *15*, R1669.
(5) Limmer, D. T.; Chandler, D. *J. Chem. Phys.* **2011**, *135*, 134503.
(6) Poole, P. H.; Sciortino, F.; Essmann, U.; Stanley, H. E. *Nature* **1992**, *360*, 324.
(7) Limmer, D. T.; Chandler, D. *J. Chem. Phys.* **2013**, *138*, 214504.
(8) Poole, P. H.; Bowles, R. K.; Saika-Voivod, I.; Sciortino, F. *J. Chem. Phys.* **2013**, *138*, 034505.
(9) Palmer, J. C.; Martelli, F.; Liu, Y.; Car, R.; Panagiotopoulos, A. Z.; Debenedetti, P. G. *Nature* **2014**, *510*, 385.
(10) Stillinger, F. H.; Rahman, A. *J. Chem. Phys.* **1974**, *60*, 1545.
(11) Liu, Y.; Panagiotopoulos, A. Z.; Debenedetti, P. G. *J. Chem. Phys.* **2009**, *131*, 104508.
(12) Brovchenko, I.; Geiger, A.; Oleinikova, A. *J. Chem. Phys.* **2005**, *123*, 044515.
(13) Harrington, S.; Poole, P. H.; Sciortino, F.; Stanley, H. E. *J. Chem. Phys.* **1997**, *107*, 7443.
(14) Berendsen, H. J. C.; Grigera, J. R.; Straatsma, T. P. *J. Phys. Chem.* **1987**, *91*, 6269.
(15) Jorgensen, W. L.; Chandrasekhar, J.; Madura, J. D.; Impey, R. W.; Klein, M. L. *J. Chem. Phys.* **1983**, *79*, 926.
(16) Horn, H. W.; Swope, W. C.; Pitera, J. W.; Madura, J. D.; Dick, T. J.; Hura, G. L.; Head-Gordon, T. *J. Chem. Phys.* **2004**, *120*, 9665.
(17) Abascal, J. L. F.; Sanz, E.; Fernàndez, R. G.; Vega, C. *J. Chem. Phys.* **2005**, *122*, 234511.
(18) Abascal, J. L. F.; Vega, C. *J. Chem. Phys.* **2005**, *123*, 234505.
(19) Vega, C.; Abascal, J. L. F. *Phys. Chem. Chem. Phys.* **2011**, *13*, 19663.
(20) Pedulla, J. M.; Vila, F.; Jordan, K. D. *J. Chem. Phys.* **1996**, *105*, 11091.
(21) Hodges, M. P.; Stone, A. J.; Xantheas, S. S. *J. Phys. Chem. A* **1997**, *101*, 9163.
(22) Ojamäe, L.; Hermansson, K. *J. Phys. Chem.* **1994**, *98*, 4271.
(23) Xantheas, S. S. *Chem. Phys.* **2000**, *258*, 225.
(24) Kumar, R.; Wang, F.-F.; Jenness, G. R.; Jordan, K. D. *J. Chem. Phys.* **2010**, *132*, 014309.
(25) Babin, V.; Medders, G. R.; Paesani, F. *J. Phys. Chem. Lett.* **2012**, *3*, 3765.
(26) Han, J.; Mazack, M. J. M.; Zhang, P.; Truhlar, D. G.; Gao, J. *J. Chem. Phys.* **2013**, *139*, 054503.
(27) Wang, L.-P.; Head-Gordon, T. L.; Ponder, J. W.; Ren, P.; Chodera, J. D.; Eastman, P. K.; Martinez, T. J.; Pande, V. S. *J. Phys. Chem. B* **2013**, *117*, 9956.

DOI: 10.1021/acs.jctc.5b00117
J. Chem. Theory Comput. 2015, 11, 2268−2277

(28) Kiss, P. T.; Baranyai, A. *J. Chem. Phys.* **2013**, *138*, 204507.
(29) Tröster, P.; Lorenzen, K.; Tavan, P. *J. Phys. Chem. B* **2014**, *118*, 1589.
(30) Fanourgakis, G. S.; Xantheas, S. S. *J. Chem. Phys.* **2008**, *128*, 074506.
(31) Wang, Y.; Huang, X.; Shepler, B. C.; Braams, B. J.; Bowman, J. M. *J. Chem. Phys.* **2011**, *134*, 094509.
(32) Bukowski, R.; Szalewicz, K.; Groenenboom, G. C.; van der Avoird, A. *Science* **2007**, *315*, 1249.
(33) Wang, Y.; Shepler, B. C.; Braams, B. J.; Bowman, J. M. *J. Chem. Phys.* **2009**, *131*, 054511.
(34) Kumar, R.; Skinner, J. L. *J. Phys. Chem. B* **2008**, *112*, 8311.
(35) Tainter, C. J.; Pieniazek, P. A.; Lin, Y.-S.; Skinner, J. L. *J. Chem. Phys.* **2011**, *134*, 184501.
(36) Pieniazek, P. A.; Tainter, C. J.; Skinner, J. L. *J. Am. Chem. Soc.* **2011**, *133*, 10360.
(37) Pieniazek, P. A.; Tainter, C. J.; Skinner, J. L. *J. Chem. Phys.* **2011**, *135*, 044701.
(38) Tainter, C. J.; Skinner, J. L. *J. Chem. Phys.* **2012**, *137*, 104304.
(39) Tainter, C. J.; Ni, Y.; Shi, L.; Skinner, J. L. *J. Phys. Chem. Lett.* **2013**, *4*, 12.
(40) Shi, L.; Ni, Y.; Drews, S. E. P.; Skinner, J. L. *J. Chem. Phys.* **2014**, *141*, 084508.
(41) Shi, L.; Gruenbaum, S. M.; Skinner, J. L. *J. Phys. Chem. B* **2012**, *116*, 13821.
(42) Ni, Y.; Skinner, J. L. *J. Chem. Phys.* **2014**, *141*, 024509.
(43) Kann, Z. R.; Skinner, J. L. *J. Chem. Phys.* **2014**, *141*, 104507.
(44) Stanley, H. E. *Introduction to Phase Transitions and Critical Phenomena*; Oxford University Press: Oxford, 1971.
(45) Huang, C.; Wikfeldt, K. T.; Tokushima, T.; Nordlund, D.; Harada, Y.; Bergmann, U.; Niebuhr, M.; Weiss, T. M.; Horikawa, Y.; Leetmaa, M.; Ljungberg, M. P.; Takahash, O.; Lenz, A.; Ojamae, L.; Lyubartsev, A. P.; Shin, S.; Pettersson, L. G. M.; Nilsson, A. *Proc. Natl. Acad. Sci. U.S.A.* **2009**, *106*, 15214.
(46) Soper, A. K.; Ricci, M. A. *Phys. Rev. Lett.* **2000**, *84*, 2881.
(47) Soper, A. K. *J. Phys. Chem. B* **2011**, *115*, 14014.
(48) Nilsson, A.; Huang, C.; Pettersson, L. G. M. *J. Mol. Liq.* **2012**, *176*, 2.
(49) Vega, C.; Abascal, J. L. F.; Nezbeda, I. *J. Chem. Phys.* **2006**, *125*, 034503.
(50) Weinhold, F.; Landis, C. *Valency and Bonding: A Natural Bond Orbital Donor-Acceptor Perspective*; Cambridge University Press: Cambridge, 2005.
(51) Hess, B.; Kutzner, C.; van der Spoel, D.; Lindahl, E. *J. Chem. Theory Comput.* **2008**, *4*, 435.
(52) van der Spoel, D.; Lindahl, E.; Hess, B.; Groenhof, G.; Mark, A. E.; Berendsen, H. J. C. *J. Comput. Chem.* **2005**, *26*, 1701.
(53) Lindahl, E.; Hess, B.; van der Spoel, D. *J. Mol. Model.* **2001**, *7*, 306.
(54) Berendsen, H. J. C.; van der Spoel, D.; van Drunen, R. *Comput. Phys. Commun.* **1995**, *91*, 43.
(55) Hayward, J.; Reimers, J. *J. Chem. Phys.* **1997**, *106*, 1518.
(56) Li, F.; Skinner, J. L. *J. Chem. Phys.* **2010**, *132*, 204505.
(57) Li, F.; Skinner, J. L. *J. Chem. Phys.* **2010**, *133*, 244504.
(58) Li, F.; Skinner, J. L. *J. Chem. Phys.* **2011**, *134*, 099901.
(59) Nosé, S. *J. Chem. Phys.* **1984**, *81*, 511.
(60) Hoover, W. G. *Phys. Rev. A* **1985**, *31*, 1695.
(61) Parrinello, M.; Rahman, A. *J. Appl. Phys.* **1981**, *52*, 7182.
(62) Allen, M. P.; Tildesley, D. J. *Computer Simulation of Liquids*; Clarendon: Oxford, 1987.
(63) Essmann, U.; Perera, L.; Berkowitz, M. L.; Darden, T.; Lee, H.; Pedersen, L. G. *J. Chem. Phys.* **1995**, *103*, 8577.
(64) Hess, B. *J. Chem. Theory Comput.* **2008**, *4*, 116.
(65) Holz, M.; Heil, S. R.; Sacco, A. *Phys. Chem. Chem. Phys.* **2000**, *2*, 4740.
(66) Dunweg, B.; Kremer, K. *J. Chem. Phys.* **1993**, *99*, 6983.
(67) Yeh, I. C.; Hummer, G. *J. Phys. Chem. B* **2004**, *108*, 15873.
(68) Miller, T. F.; Manolopoulos, D. E. *J. Chem. Phys.* **2005**, *123*, 154504.
(69) Vega, C.; Abascal, J. L. F. *J. Chem. Phys.* **2005**, *123*, 144504.
(70) Kiss, P. T.; Baranyai, A. *J. Chem. Phys.* **2009**, *131*, 204310.
(71) Chialvo, A. A.; Bartok, A.; Baranyai, A. *J. Mol. Liq.* **2006**, *129*, 120.
(72) Bellissent-Funel, M.-C.; Chen, S. H.; Zanotti, J.-M. *Phys. Rev. E* **1995**, *51*, 4558.
(73) Novikov, A. G.; Van'kov, A. A.; Gosteva, L. S. *J. Struct. Chem.* **1990**, *31*, 77.
(74) Egorov, S. A.; Everitt, K. F.; Skinner, J. L. *J. Phys. Chem. A* **1999**, *103*, 9494.
(75) Lawrence, C. P.; Nakayama, A.; Makri, N.; Skinner, J. L. *J. Chem. Phys.* **2004**, *120*, 6621.
(76) Medders, G. R.; Babin, V.; Paesani, F. *J. Chem. Theory Comput.* **2014**, *10*, 2906.
(77) Bertie, J. E.; Lan, Z. *Appl. Spectrosc.* **1996**, *50*, 1047.
(78) McQuarrie, D. A. *Statistical Mechanics*; Harper and Row: New York, 1976.
(79) Saul, A.; Wagner, W. *J. Phys. Chem. Ref. Data* **1989**, *18*, 1537.
(80) Ropp, J.; Lawrence, C.; Farrar, T. C.; Skinner, J. L. *J. Am. Chem. Soc.* **2001**, *123*, 8047.
(81) Jonas, J.; DeFries, T.; Wilbur, D. J. *J. Chem. Phys.* **1976**, *65*, 582.
(82) Wegner, F. *J. Phys. Rev. B* **1972**, *5*, 4529.
(83) Ley-Koo, M.; Green, M. S. *Phys. Rev. A* **1981**, *23*, 2650.
(84) Rowlinson, J. S.; Swinton, R. L. *Liquids and Liquid Mixtures*; Butterworths: London, 1982.
(85) Soper, A. K. *Chem. Phys.* **2000**, *258*, 121.
(86) IAPWS Web site. http://www.iapws.org/relguide/IAPWS-95.html (accessed October 15, 2014).
(87) Bruges, E. A.; Gibson, M. R. *J. Mech. Eng. Sci.* **1969**, *11*, 189.
(88) Lamb, W. J.; Hoffman, G. A.; Jonas, J. *J. Chem. Phys.* **1981**, *74*, 6875.
(89) Krynicki, K.; Green, C. D.; Sawyer, D. W. *Faraday Discuss. Chem. Soc.* **1978**, *66*, 199.
(90) Kell, G. S. *J. Chem. Eng. Data* **1975**, *20*, 97.
(91) Vega, C.; Sanz, E.; Abascal, J. L. F. *J. Chem. Phys.* **2005**, *122*, 114507.
(92) Vega, C.; de Miguel, E. *J. Chem. Phys.* **2007**, *126*, 154707.
(93) Harvey, A. H.; Lemmon, E. W. *J. Phys. Chem. Ref. Data* **2004**, *33*, 369.
(94) Kell, G. S.; McLaurin, G. E.; Whalley, E. *Proc. R. Soc. London, Ser. A* **1989**, *425*, 49.
(95) IAPWS Web site. http://www.iapws.org/relguide/LiquidWater.pdf (accessed October 15, 2014).
(96) Wagner, W.; Saul, A.; Prub, A. *J. Phys. Chem. Ref. Data* **1994**, *23*, 515.

DOI: 10.1021/acs.jctc.5b00117
J. Chem. Theory Comput. 2015, 11, 2268−2277